Case Studies in Construction Materials 16 (2022) e00948

Contents lists available at ScienceDirect

Case Studies in Construction Materials

journal homepage: www.elsevier.com/locate/cscm

Case study

Plastic and early-age shrinkage of ultra-high performance concrete (UHPC): Experimental study of the effect of water to binder ratios, silica fume dosages under controlled curing conditions

Ming Sun, Terry Bennett *, Phillip Visintin

School of Civil, Environmental and Mining Engineering, The University of Adelaide, South Australia 5005, Australia

ARTICLE INFO

Keywords:
Ultra-high performance concrete
Autogenous shrinkage
Water to binder ratio
Silica fume
Capillary tension

ABSTRACT

The magnitude of early age shrinkage of Ultra High Performance Concrete (UHPC) is markedly different from normal and high strength concretes. A series of experiments were performed to determine the influence of water to binder ratio and silica fume content on the rate of hydration, stiffness development, chemical and external shrinkage under both sealed and unsealed conditions. Experimental apparatus, designed for shrinkage in normal strength concretes, were adapted to accommodate the larger volume changes and minimise the influence of boundary restraint. Continuously monitored internal temperature, and relative humidity conditions, along with periodic measurements of hydration degree and stiffness are used to elucidate the volumetric deformation mechanisms. Results, from as early as three hours after water addition demonstrate significant volumetric changes occurring in the early plastic state of the material.

1. Introduction

Ultra-high performance concrete (UHPC) is characterised by its superior compressive strength and high durability, these characteristics arise from several key mix design parameters, including low water to binder ratio (w/b) and high binder content (cement and silica fume) [1–6]. Although possessing several highly desirable properties, UHPC also undergoes substantial time-dependent deformations due to shrinkage [2,6–10]. Unlike normal strength concrete in which shrinkage deformations occur predominately from drying [11], UHPC can have far larger deformations arising from autogenous shrinkage [6,12], particularly at the early ages of strength development. An understanding of early age shrinkage is therefore essential because defects formed in these early stages, when tensile strength is low, are likely to initiate cracking at later ages [13].

In normal strength concrete, total shrinkage is typically dominated by drying shrinkage which occurs as the pore environment comes into equilibrium with the external relative humidity and temperature over long time periods [14]. Conversely, it is has been shown that UHPC shrinkage is predominately driven by early age mechanisms including those associated with the initial plastic stage of concrete [15]. That is, early age shrinkage is predominately driven by the chemical shrinkage and evaporation of mix water occurring before the formation of solid skeleton [15–17], followed by capillary stresses in the pore water which link self-desiccation and autogenous shrinkage [18,19].

Several key parameters which warrant further investigation are identified from literature. The influence of water to cement ratios (w/c) were studied by Eppers and Müller [20] who performed experiments to measure autogenous shrinkage of UHPC and found

* Corresponding author.
E-mail address: terry.bennett@adelaide.edu.au (T. Bennett).

https://doi.org/10.1016/j.cscm.2022.e00948
Received 14 December 2021; Received in revised form 6 February 2022; Accepted 12 February 2022
Available online 14 February 2022

Table 1
Existing studies on UHPC shrinkage measured from plastic stage without the effect of fibres (C=cement, SF=silica fume, FA=fly ash, W=water, SP=superplasticizer, HRWRA=high range water reducing agent, LS=limestone, VD=volume deformation, AS=autogenous shrinkage, TS=total shrinkage).

Authors	Mix design	Fibre type, dosage	w/b or w/c	Silica fume content	Studied parameters	Testing conditions	Specimen size (mm)	Measurement start time	Shrinkage type	Main findings
Zhang, Liu and Wang [26]	C (P.O. 52.5), SF, FA, Silica sand, Steel fibre, W, SP	Unknown steel fibre type, 0%, 1%, 1.5% and 2.5% vol	w/b= 0.18	12.7% mass of binder	Fibre dosages= 0%, 1%, 1.5% and 2.5% vol	T ≈ 20℃	40 * 60 * 1000	Casting	AS	The increase in fibre dosage resulted in decreased autogenous shrinkage.
Li et al. [3]	C (P.O. 42.5), Quartz sand, Silica flour, SF, FA, W, Reinforcing bar	Reinforcing bar (4 *dia 8 mm, L 512 mm; 4 *dia 10 mm, L 512 mm; 4 *dia 12 mm, L 512 mm)	w/b= 0.18	16.7% mass of binder	Reinforcement ratios= 0%, 2%, 3.14% and 4.52%	Heat treatment (T = 20℃-90℃-20℃)	100 * 100 * 515	Casting	AS without thermal expansion	The increased reinforcement ratios leaded to decreased autogenous shrinkage.
Wu, Shi and Khayat [27]	C, Sand, Silica fume, W, SP, Steel fibres	Straight fibre (dia 0.2 mm, L 13 mm), Corrugated fibre (dia 0.2 mm, L 13 mm), Hooked fibre (dia 0.2 mm, L 13 mm), 0%, 1% and 3% vol	w/b= 0.18	20% mass of binder	Straight fibre (dia 0.2 mm, L 13 mm), Corrugated fibre (dia 0.2 mm, L 13 mm) and Hooked fibre (dia 0.2 mm, L 13 mm) type Straight fibre dosages= 0%, 1%, 2% and 3%	T = 20℃	Corrugated tube	Casting	AS	The increase in fibre dosages decreased autogenous shrinkage. Corrugated fibres were more efficient in reducing autogenous shrinkage and hooked fibres were event better.
Wang et al. [28]	C, SF, Filler, Silica sand, W, SP, Steel fibres, High performance calcium sulphoaluminate	Straight steel fibres (dia 0.2 mm, L16mm), 1% and 2% vol	w/b= 0.19	23% mass of binder	High performance calcium sulphoaluminate dosages= 0%, 3% and 6% mass of binder	T = 20℃, RH= 50%	100 * 100 * 515	Casting	TS	The total shrinkage decreased accordingly with the increase in high performance calcium sulphoaluminate dosages.
	C, SF, Filler, Silica sand, W, SP, Steel fibres	Straight steel fibres (dia 0.2 mm, L16mm), 1% and 2% vol	w/b= 0.19	23% mass of binder	Steel fibre dosages= 1% and 2% vol	T = 20℃, RH= 50%	100 * 100 * 515	Casting	TS	The increase in fibre dosage resulted in reduced total shrinkage.

(*continued on next page*)

Table 1 (*continued*)

Authors	Mix design	Fibre type, dosage	w/b or w/c	Silica fume content	Studied parameters	Testing conditions	Specimen size (mm)	Measurement start time	Shrinkage type	Main findings
Liu et al. [29]	C (type I), slag cement, SF, Silica sand (300 μm, 1000 μm), W, SP	No fibre	w/b= 0.18	20% mass of binder	Slag cement dosages as C replacement= 0%, 25%, 50%, 65%	Unknown	60 * 100 * 1000	3–4 h after water addition	VD	A higher replacement ratio of slag cement resulted in smaller early-age and larger long-term autogenous shrinkage.
Yang et al. [30]	C (CEM I), Phosphorous slag, FA, SF, Sand (0–0.6 mm, 0.6–1.25 mm), W, HRWRA	No fibre	w/b= 0.17	13.2% mass of binder	Phosphorous slag dosages as C replacement= 0%, 10%, 20%, 30%, 40%, 50%	T = 20℃	100 * 100 * 515	Casting	AS	Autogenous shrinkage decreased with the rise of phosphorous slag replacement ratio.
Yang et al. [31]	C (type I), LS powder, FA, SF, Sand (0–0.6 mm), W, SP	No fibre	w/b= 0.16	12.3% mass of binder	LS powder dosages as C replacement= 0%, 22.22%, 44.44% mass of C	T = 20℃	100 * 100 * 515	Casting	AS	The increase in LS powder decreased UHPC autogenous shrinkage.
	C (type I), Basalt powder, FA, SF, Sand (0–0.6 mm), W, SP	No fibre	w/b= 0.16	12.3% mass of binder	Basalt powder dosages as C replacement= 0%, 22.22%, 44.44% mass of C	T = 20℃	100 * 100 * 515	Casting	AS	The increase in basalt powder decreased UHPC autogenous shrinkage.

Table 2
Mix proportions by weight of UHPC.

Mix ID	*w/b*	SF replacement ratio	Cement	Silica fume	Water	Sand	SP
WB15-SF10	0.15	10%	0.9	0.1	0.115	1	0.05
WB15-SF15		15%	0.85	0.15	0.115	1	0.05
WB15-SF20		20%	0.8	0.2	0.115	1	0.05
WB17-SF10	0.17	10%	0.9	0.1	0.135	1	0.05
WB17-SF15		15%	0.85	0.15	0.135	1	0.05
WB17-SF20		20%	0.8	0.2	0.135	1	0.05
WB19-SF10	0.19	10%	0.9	0.1	0.155	1	0.05
WB19-SF15		15%	0.85	0.15	0.155	1	0.05
WB19-SF20		20%	0.8	0.2	0.155	1	0.05

shrinkage to increase with increasing cement content and decreasing water content. It was also found that cement with higher C_3A content resulted in greater shrinkage strains.

Curing temperature can also significantly affect autogenous shrinkage and is particularly important for UHPC, as it commonly cured at elevated external temperature [3,9,21,22] which leads to accelerated hydration reactions [22]. The accelerated rate of hydration reactions can also be self-inducing, as a result of the exothermal heat produced by the hydration process. The consumption of water in the reactions leads to shrinkage from capillary action. This effect is particularly prominent at early ages, given that chemical shrinkage is a main driving force for shrinkage before solid skeleton formation [23].

The production of UHPC generally requires the use of supplementary cementitious materials (SCMs) that also have an effect on the magnitude of early age shrinkage. It was found by Shen et al. [9] that silica fume can increase autogenous shrinkage due to both the reduction of pore sizes and pozzolanic reactions; however, Eppers and Müller [20] found no clear correlation between silica fume content and autogenous shrinkage. This discrepancy suggests further study is required.

When used as a silica fume replacement, ground granulated blast furnace slag (GGBFS) can reduce autogenous shrinkage because its larger grain size, compared with silica fume, leads to a larger pore size and therefore reduced capillary action [1]. However, when used as a replacement for cement, the smaller grain size of GGBFS, compared to cement, has been shown to increase autogenous shrinkage [22]. Termkhajornkit et al. [24] demonstrated that unhydrated fly ash can reduce autogenous shrinkage by acting as a restraint. However in contrast, Tazawa [25] found that very fine fly ash can give rise to autogenous shrinkage, through both pore size reduction and pozzolanic reaction. Given the role of SCMs can influence the competing mechanism of capillary action and stiffness further research is also required to understand the impact of SCMs at a range of different binder (cement and silica fume) replacement ratios.

The number of studies of very early-age shrinkage, measured from the plastic stage, of UHPC is limited, and as shown in Table 1, reduces further again when filtering experiments performed without fibres.

Very early age shrinkage including the influence of various fibre volumes was studied by Zhang, Liu and Wang [26] investigated the restraint effect of steel fibre dosage on UHPC autogenous shrinkage, measured from casting. Lim et al. [32] measured UHPC autogenous shrinkage from casting and studied the effects of silica sand, GGBFS and carbon nanofibers. Li et al. [3] observed the impacts of reinforcement and heat treatment on UHPC autogenous shrinkage, measured from the time of casting. Wang et al. [28] and Wu et al. [27] investigated the effects steel fibre dosage on UHPC total shrinkage, measured from casting.

Liu et al. [29] studied the effect of slag cement by measuring volume deformation of UHPC beginning 3–4 h after water addition, and identified distinct shrinkage development stages and observed an increasing effect of slag cement on UHPC autogenous shrinkage.

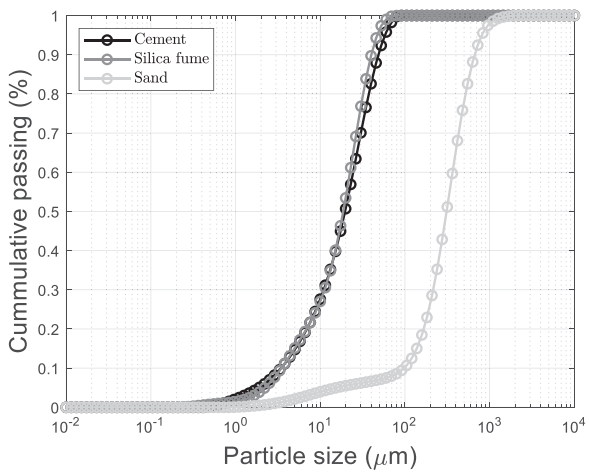

Fig. 1. Particle size distributions of cement, silica fume and sand.

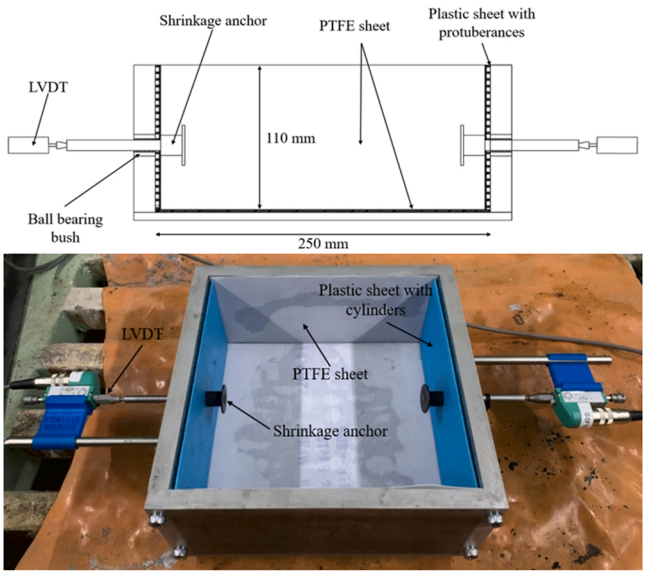

Fig. 2. Moisture-related shrinkage measurement set-up.

Yang et al. [30] and Yang et al. [31] studied the effects of phosphorous slag, limestone powder and basalt powder on UHPC autogenous shrinkage from casting, utilising non-contact sensors. From Table 1, it can be seen that there is no study on the effects of water to binder ratios and silica fume dosages on UHPC early-age shrinkage, measured from plastic stage.

To further understand the effects of SCM (supplementary cementitious materials) replacement and water to binder ratio on the plastic and early age shrinkage of UHPC, the results of a series of sealed and unsealed shrinkage experiments are reported here. The material is cast directly in to bespoke moulds, which are also used as the basis to measure volumetric changes occurring in the early plastic state and on through the formation of the solid skeleton. To enable decomposition of the different components of shrinkage chemical shrinkage was concurrently measured for the same mixes from 3 h up to 7 days.

Temperature and humidity sensors were embedded in samples to monitor the internal environment, both spatially and temporally. The development of material stiffness and the reaction degree were also measured in parallel in order to elucidate the shrinkage mechanisms and to provide the required inputs to validate or employ in models.

The mix design and methodology are described in Section 2, the experimental results and corresponding data analysis can be seen in Section 3, further discussion and data synthesis are shown in Section 4, followed by conclusions in Section 5.

2. Material and methods

In order to understand the mechanisms of UHPC early-age shrinkage and decompose the different components of shrinkage, several parameters need to be measured experimentally, these include shrinkage under sealed and unsealed conditions, relative humidity (RH), temperature, degree of reaction, chemical shrinkage, and bulk modulus.

A refrigerated thermal and humidity controlled cabinet was used to control the temperature at 25℃ and 50% relative humidity for the shrinkage tests and sample curing described in this section. The cabinet (Humiditherm TRH-850) had a temperature range of 5℃ to 60℃ and humidity range of 10–95% with accuracy of ± 0.2℃ and 1% *RH*.

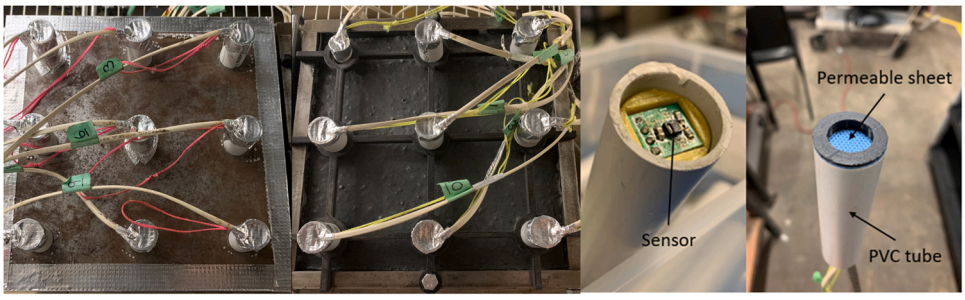

Fig. 3. Temperature and relative humidity measurement sensor and set-up.

2.1. Mix design

The shrinkage behaviour of UHPC is governed by the water and silica fume content. For example, silica fume can refine pore size to increase shrinkage via capillary action [7] and the pozzolanic reaction of silica fume has larger chemical shrinkage (approximately 20 mL/100 g) than Portland cement (approximately 6.4 mL/100 g) [7,16]. The water content also affects cement hydration, self-desiccation and drying all of which influence shrinkage [7]. Therefore, nine mix designs with different w/b ratios and different silica fume replacement ratios were tested in this research. The base mix design with a weight ratio of cement:silica fume:water:sand of 0.79:0.21:0.13:1 was obtained from Xie et al. [6] and parametric variations as shown in Table 2 were then introduced. The parametric variations in w/b and silica fume content of UHPC were chosen to have wide enough range to investigate their effects on UHPC shrinkage and simultaneously ensure adequate workability at the same time. Therefore, parameter changes vary around the base mix design to guarantee reliable UHPC mix design. In Table 2, each mix is given an ID according to its water to binder ratio and proportional weight of silica fume. For example, mix WB15-SF10 has a w/b of 0.15 and a silica fume replacement ratio of 0.1.

Two types of cementitious binder were used, sulphate resisting cement (Type SR) conforming to Australian standard AS3972–2010 [33] and densified amorphous silica fume conforming to Australian standard AS/NZS 3582.3:2016 [34]. According to the product data sheet [35], the manufacturer reported components of sulphate resisting cement are 30%–50% Portland cement clinker, 50–70% ground granulated blast furnace slag (GGBFS) and 2–5% gypsum by weight. The silica fume components have over 89.6% silicon dioxide SiO_2 and the other chemical components can be seen in the manufacturer product data sheet [36]. A natural washed river sand was used as the fine aggregate for all UHPC mixes. The particle size distributions of cement, silica fume and sand, measured by Malvern

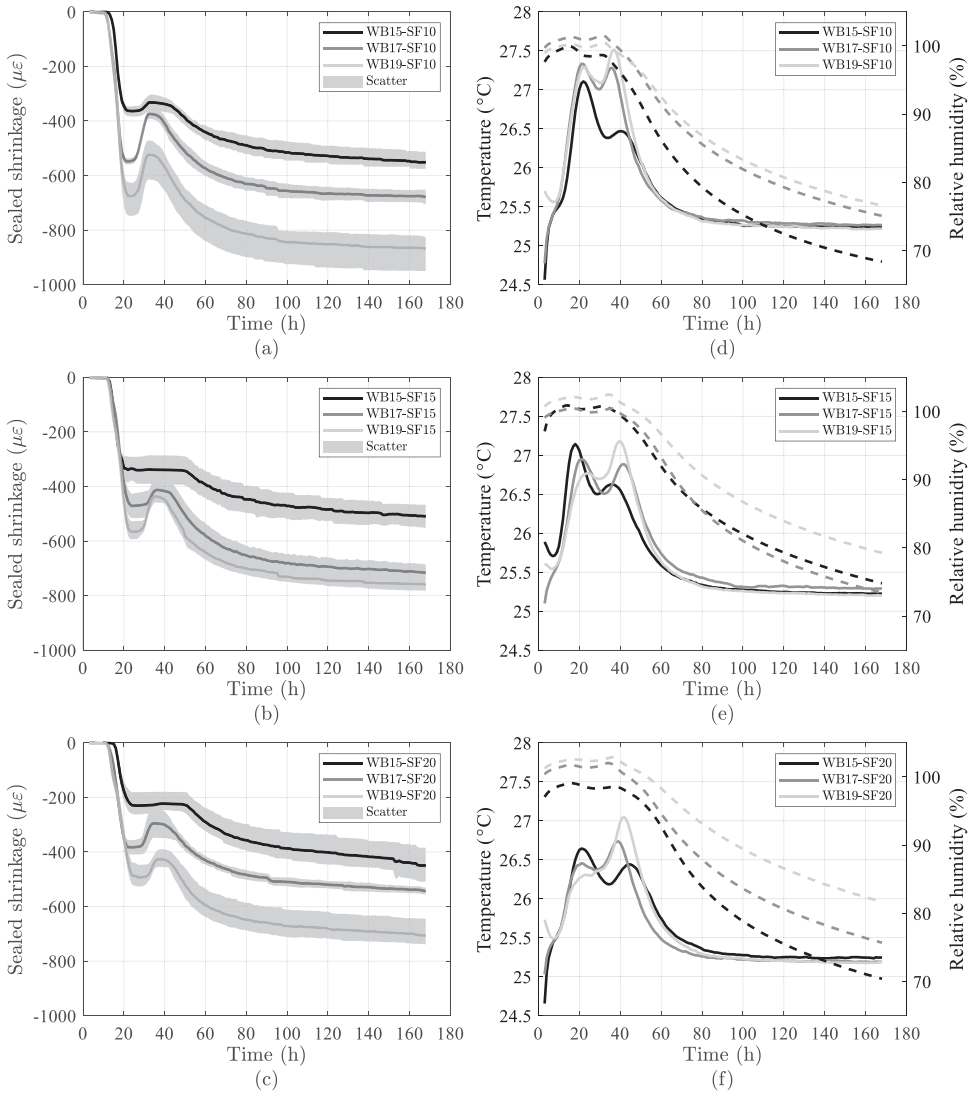

Fig. 4. The effect of w/b and silica fume ratio on sealed shrinkage (left), temperature and relative humidity (right), recorded from 3 h after water addition.

Mastersizer 2000 particle size analyser are shown in Fig. 1. A high range water reducing superplasticizer with retarder was used, its water content (approximately 70%) was considered to be available for hydration reaction by adding to the total water content in the mix design (i.e. the water to binder ratio was calculated based on added water content in Table 2 and water content in superplasticizer). Thermal gravity analysis (TGA) and chemical shrinkage measurements were performed on UHPC paste without the inert sand.

Mixing was performed in a pan mixer, with 165 kg of concrete produced for each mix design. The dry materials, including cement, silica fume and sand were placed into the mixer and mixed for 5 min, followed by slow addition of water. Superplasticizer was then slowly added. The mixing process was continued for additional 30 min after the water and superplasticizer was added to ensure workability. For TGA and chemical shrinkage testing, 2 kg of UHPC paste (without sand) was batched in a bench-top mixer.

2.2. Shrinkage measurement

To measure early-age shrinkage, a mould with walls that can support concrete in its plastic phase is required. A total of six steel moulds shown in Fig. 2 were used, three with an open top were for shrinkage measurement under drying conditions and three with a sealed top were for shrinkage measurement under sealed conditions.

The design of the mould in Fig. 2 is based on previous tests [37–43] with modifications made to the dimensions, shrinkage anchors and materials used between the sample and box walls to ensure accurate measurement at early-ages. The dimensions of the box was 250 × 250 × 110 mm and the plan area was designed to be square in shape to minimise the effect of wall friction restraint. The box

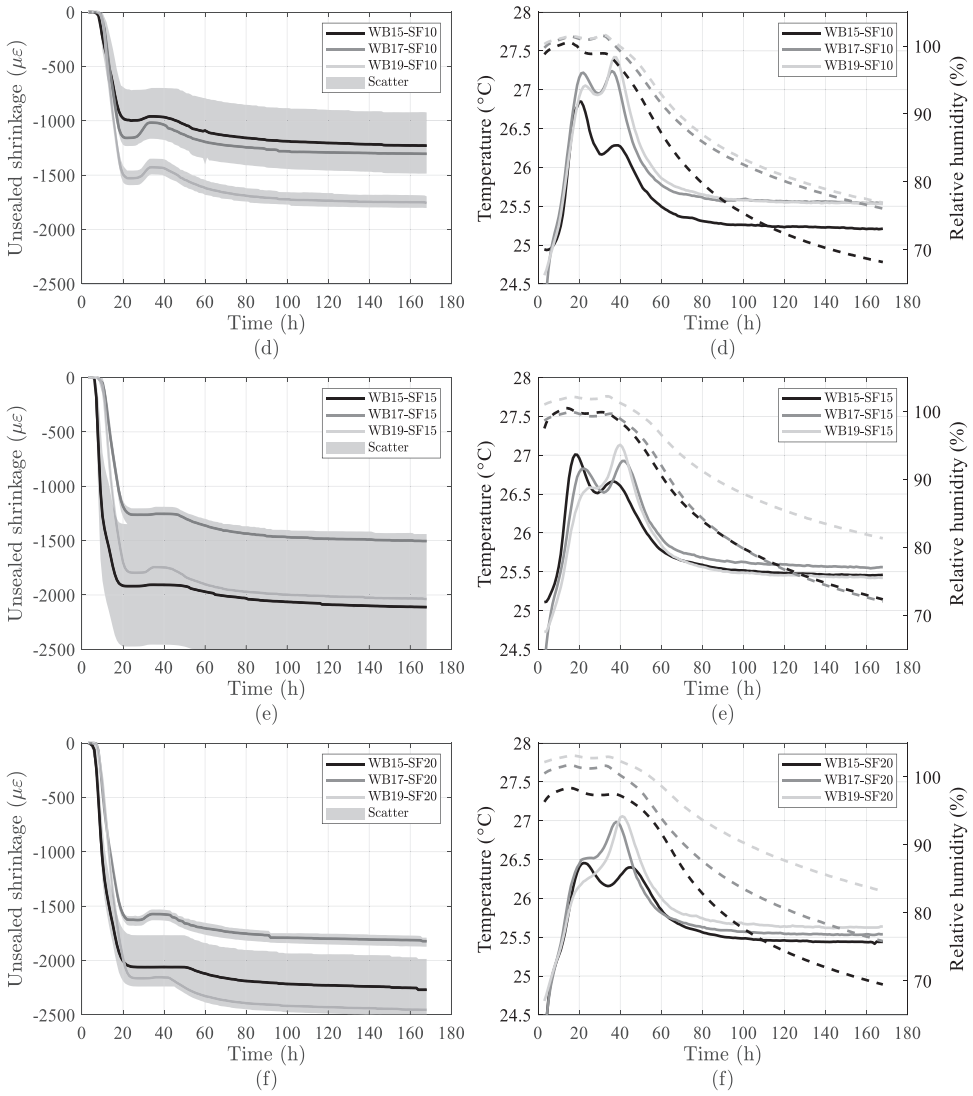

Fig. 5. The effect of w/b and silica fume ratio on unsealed shrinkage (left), temperature and relative humidity (right) recorded from 3 h after water addition.

length ensures that the shrinking distance is large enough to be accurately measured by LVDTs with stroke length of 10 mm and accuracy of ± 0.3%. The square shape is also beneficial to spatial distribution measurement of relative humidity and temperature described in Section 2.3. The mould height was designed to be 10 mm higher than the sample size to ensure that the concrete did not come into contact with, and potentially adhere to, the sealing cover used in shrinkage measurements under sealed conditions. Furthermore, to improve the seal between the mould and the environment, aluminium foil tape was applied to seal the edges of the cover.

Two shrinkage anchors connected to LVDTs (Fig. 2) were placed at two opposite sides of each box, these were supported by ball bearing bushes to reduce friction. The distance between shrinkage anchors and the bottom of the box was 50 mm. Each shrinkage anchor had an enlarged end (30 mm diameter) and was placed 20 mm into the sample to ensure that it was well supported by UHPC. In order to eliminate differential displacement caused by sliding between sample and the anchor, the calculation of shrinkage is based on the net distance between two anchor ends. The bottom and two sliding sides of each mould were cover by PTFE sheet to reduce friction. The two sides supporting shrinkage anchors were covered by 3D printed plastic sheet, which had many small protuberances to avoid sticking between sample and walls.

After placing the concrete, all six moulds were stored in the temperature and humidity cabinet until the completion of the testing period. Measurements commenced 3 h after the addition of water, for a total duration of 7 days.

2.3. Relative humidity and temperature measurement

Two steel moulds with the same dimensions as the shrinkage moulds, but without shrinkage anchors were used to measure concrete relative humidity and temperature, as shown in Fig. 3(a). The mould on the left was used for sealed condition measurement, with a steel plate cover sealing UHPC and supporting the sensors. The right one was for unsealed condition measurement, with a grid added to

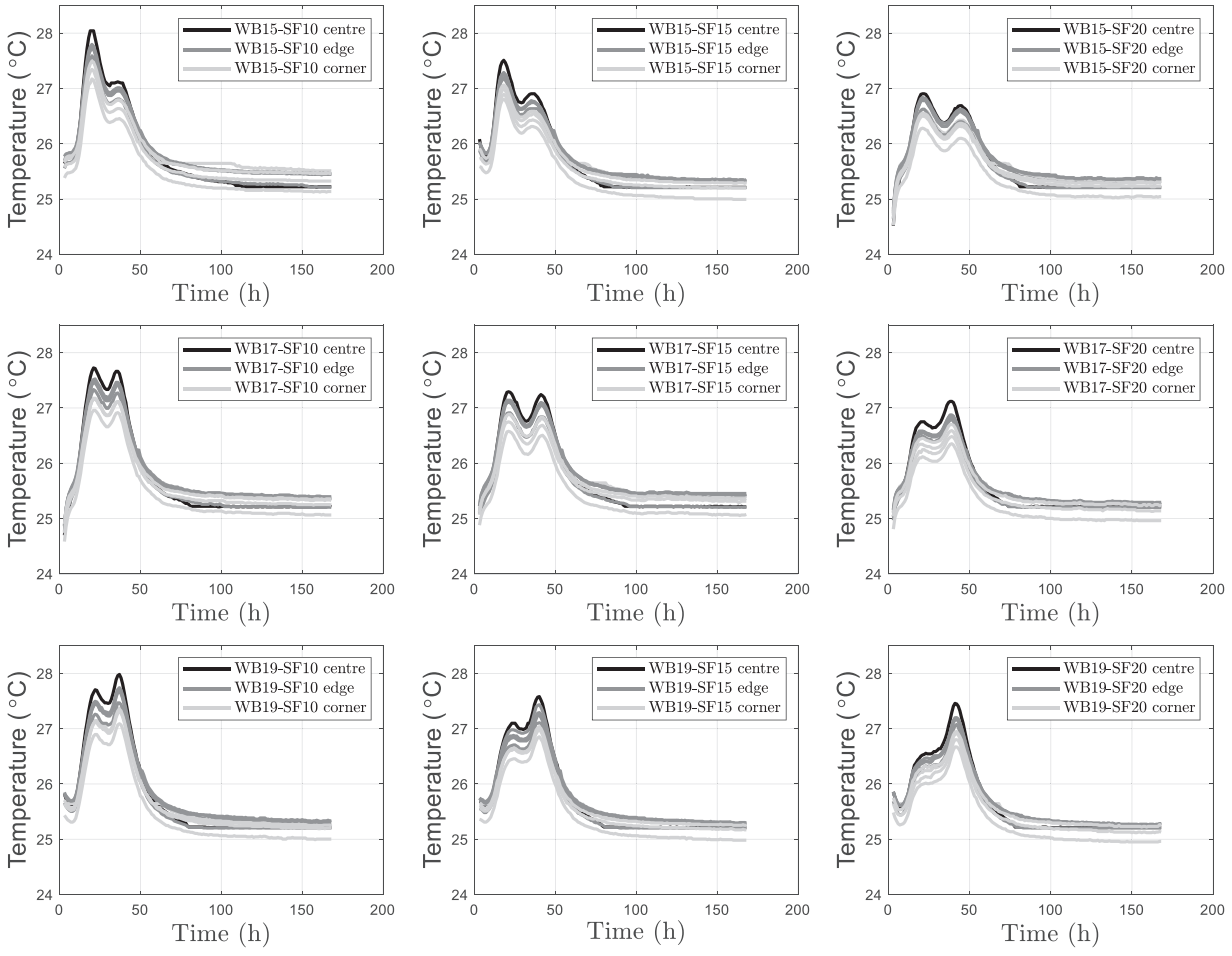

Fig. 6. Internal temperature change of each mix design under sealed (a) and unsealed (b) boundary conditions, recorded from 3 h after water addition.

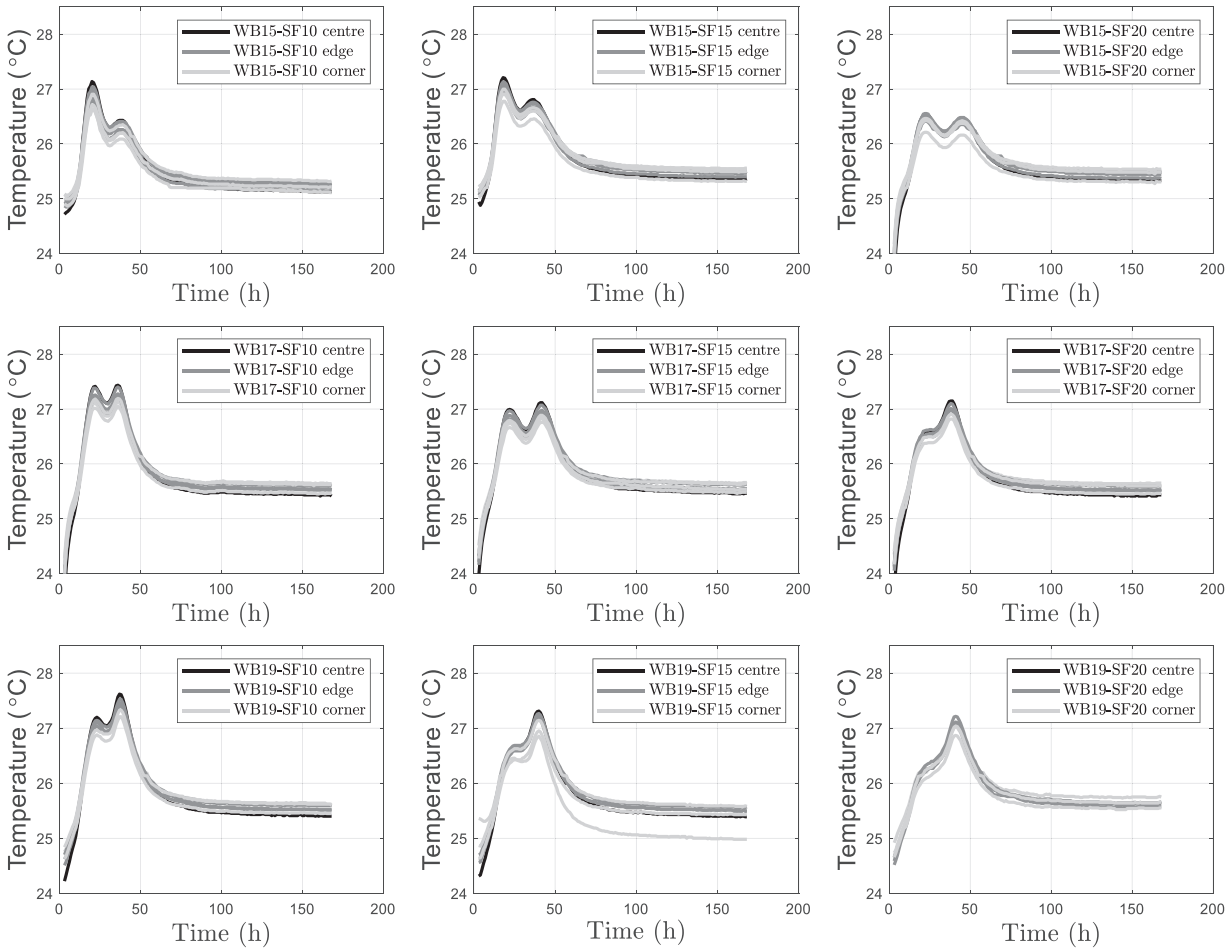

(b): Unsealed boundary conditions

Fig. 6. (*continued*).

support sensors and ensure the top surface of UHPC was exposed. Relative humidity and temperature were measured at 9 different positions at the mid-height of the UHPC sample. The distance between centres of sensors shown in Fig. 3(a) was 94 mm. As with the shrinkage samples, once the UHPC was cast into the mould, they were placed into the temperature and humidity cabinet and measurements were recorded starting from 3 h after water addition and ending at 7 days.

The digital sensors used to simultaneously measure relative humidity and temperature (model SHT21) had an operational range of −40–125 ℃ and relative humidity operation range of 0%–100%. The accuracies of relative humidity and temperature are 2% and 0.3℃ respectively. In order to hold the sensors into position, each sensor was inserted at one end of a PVC tube and the tube was inserted vertically into the UHPC sample. To isolate the sensors from liquid water, a permeable sheet that allowed water vapour to pass but not liquid water was applied to the end of the sensor tube and sealed in place with a rubber O-rings and wax [Fig. 3(b)]. The open top of the opposite side of the tube was sealed by aluminium foil tape to further prevent moisture evaporation into the environment [Fig. 3(b)].

2.4. Thermal gravity analysis

Thermal gravity analysis (TGA) was used to estimate the reaction degree of UHPC at different ages by assessing the non-evaporable water content. For each measurement at day 1 and 3, less than 10 mg sample was firstly ground and then heated from 30℃ to 1000℃ at the rate of 10℃/min in nitrogen atmosphere using a Mettler Toledo TGA testing machine. The non-evaporable water content W_B was then calculated from the weight loss of the sample, as given in Eq. (1) [44].

$$W_B(\%) = Ldh + Ldx + 0.41(Ldc - Ldc_a) \tag{1}$$

where *Ldh* represents dehydration reaction typically within the temperature range of 105–400℃, *Ldx* is the dehydroxylation of

Portlandite typically occurring between 400 and 600°C, *Ldc* is decarbonation of $CaCO_3$ typically within the range of 600–800°C [45], and Ldc_a is the carbonation of anhydrous materials, including dry cement and silica fume. In this test, the temperature range of dehydroxylation was estimated to be 300–500°C based on the derivative thermogravimetric curve (DTG). The weight change of an empty crucible was also measured and subtracted from the UHPC paste results for calibration. Once the non-evaporable water content is known, the degree of reaction α is:

$$\alpha = \frac{W_B}{W_{B\infty}} \times 100\% \tag{2}$$

where, $W_{B\infty}$ is the ultimate non-evaporable water content at full hydration. The value of $W_{B\infty}$ was chosen to be 0.23, which is $W_{B\infty}$ for Ordinary Portland Cement (OPC) paste, assuming supplementary cementitious materials (SCMs) have limited effect on this value. This is because the type SR cement used in this paper can be regarded as Portland cement with GGBFS and silica fume addition, based on its components. Monteagudo et al. [44] obtained this value for OPC, OPC with 20% BFS and OPC with 10% silica fume addition based on different methods and found the addition of SCMs does not significantly alter the degree of reaction. Deboucha et al. [45] studied hydration degree of cement paste with BFS and limestone filler additions, assuming $W_{B\infty}$ of binder is similar to that of pure cement. In addition, Xie et al. [6] also adopted 0.23 for their type SR cement with silica fume addition mixes.

2.5. Chemical shrinkage measurement

Chemical shrinkage of UHPC paste was measured using a method adapted from ASTM C1608–07 [46]. A 500 mL Erlenmeyer flask with a measuring pipette extending outside of the vessel to capture the sample volume changes was used. Approximately 50 g of UHPC paste was placed into the Erlenmeyer flask, and paraffin oil was carefully added to seal the sample. In this study, two samples were

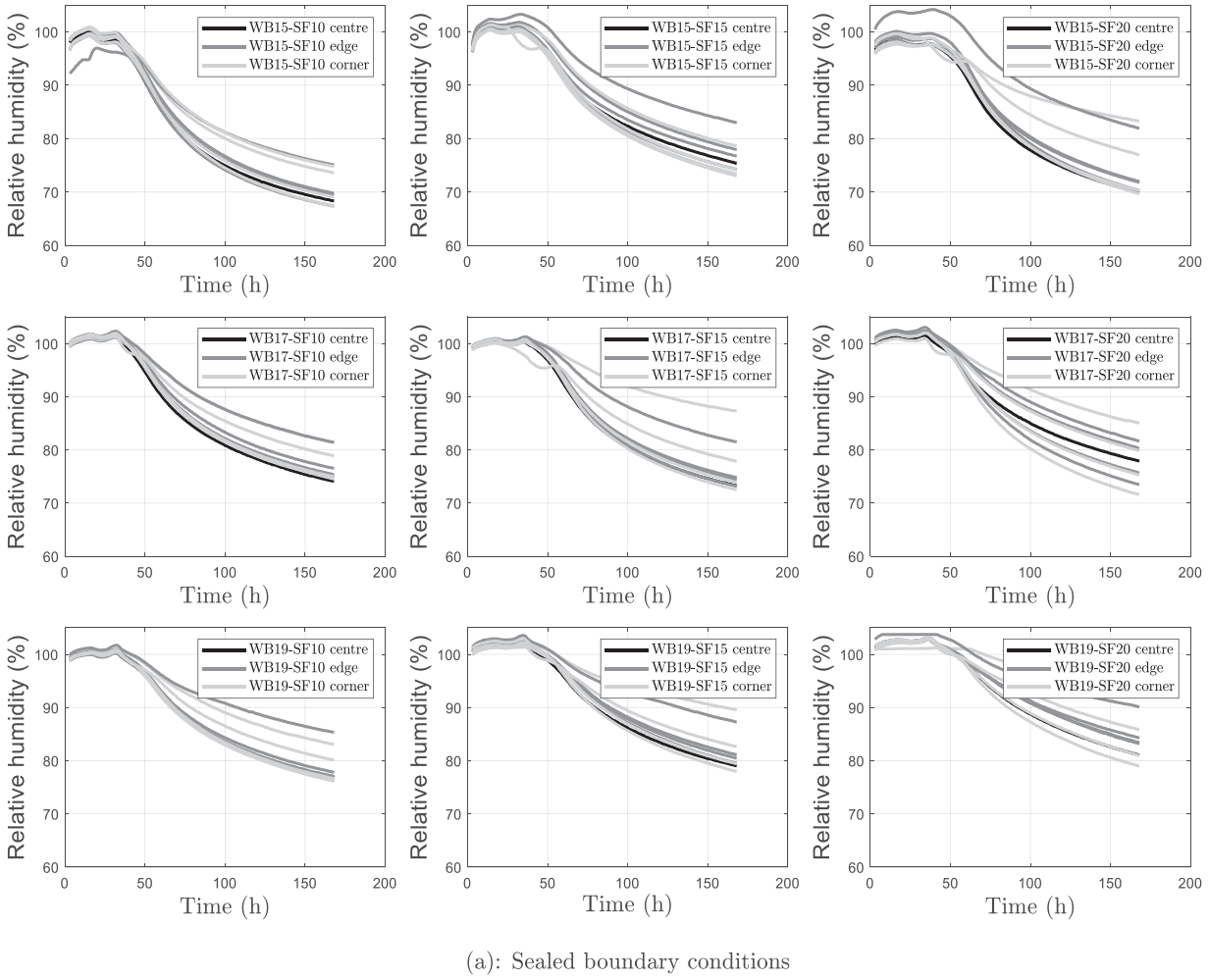

Fig. 7. Spatial distribution of internal relative humidity of each mix design under sealed (a) and unsealed (b) boundary conditions, recorded from 3 h after water addition.

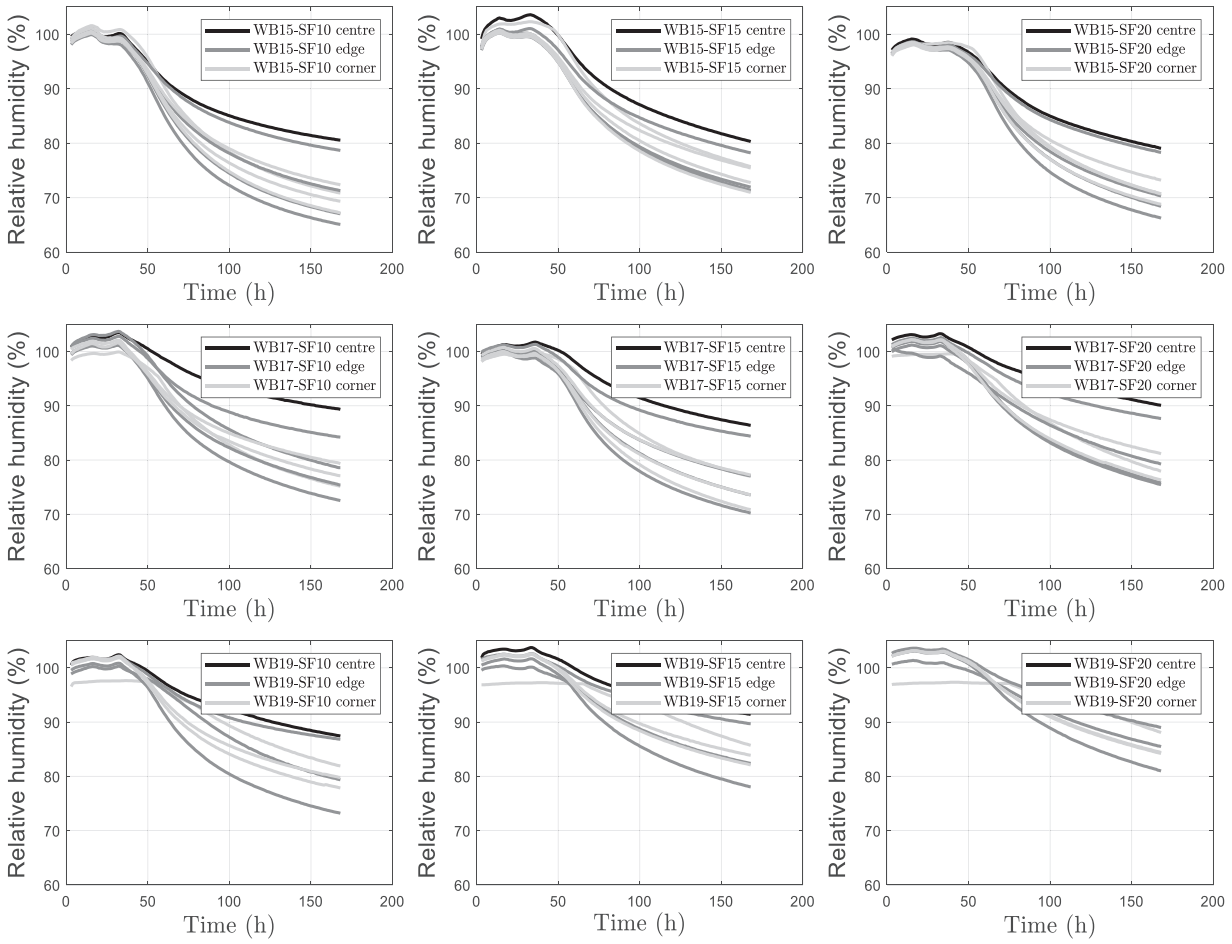

(b): Unsealed boundary conditions

Fig. 7. (*continued*).

measured simultaneously for each mix design with the measurements commencing 3 h after water addition and continuing until 7 days. A GoPro camera was used to record the liquid level change every hour over this period.

The 500 *mL* Erlenmeyer flask was chosen because it had a broad base, which is beneficial as it increases the contact area between UHPC paste and paraffin oil. The enlarged contact area and the thin sample thickness (3–5 mm) acts to accelerate the penetration of paraffin oil, reducing restraint from the flask glass and avoiding self-desiccation [47]. For normal strength cement, a pipette with 10 mL capacity is selected [47], to accurately measure the volume change encountered with UHPC samples, the pipette with 2 mL capacity and 0.01 mL graduations were used to accommodate less water, hydration reaction, and chemical shrinkage.

2.6. Stiffness and strength measurement

Bulk modulus K can be calculated from Young's modulus E and Poisson's ratio ν by Eq. (3).

$$K = \frac{E}{3(1-2\nu)} \tag{3}$$

Therefore, Young's modulus and Poisson's ratio were measured for each mix design at 48, 96 and 168 h after water addition using 75 mm × 150 mm cylinders. The cylinders remained in the mould until the start of each measurement to simulate the environment of the shrinkage mould. In order to examine the effect of drying on bulk modulus, samples were divided into two groups of three cylinders, which were either sealed or unsealed at the top surface. For testing, two cylinders from each group were used for strength measurement according to ASTM C39 [48] and the third to measure Young's modulus and Poisson's ratio according to ASTM C469 [49]. The measurement of Young's modulus and Poisson's ratio was accomplished by two axial extensometers and one circumferential extensometer, respectively.

3. Experimental results and discussion

3.1. Shrinkage

The experimentally measured data are presented and discussed in this section. The measured early-age shrinkage cannot be directly identified as autogenous or total shrinkage. That is, measured shrinkage under both sealed and unsealed boundary conditions is a combination of different mechanisms for low w/b ratio concretes, as elaborated in the following sections. Therefore, the measured shrinkage in this paper was named according to the testing conditions, which are sealed and unsealed shrinkage. It should be noted that chemical shrinkage generally refers to micro internal volume reduction; however, it can also affect macro external volume reduction [41,43]. Therefore, the term 'converted chemical shrinkage' was used to describe external shrinkage caused by chemical shrinkage.

3.1.1. Shrinkage under sealed boundary conditions

The effect of w/b and silica fume dosage on sealed shrinkage measured from 3 h after water addition can be seen in Fig. 4(a), (b) and (c) with solid lines indicating the average values of the three specimens measured and the full scatter shown by the grey shaded area. The corresponding internal temperature and relative humidity change can be seen in Fig. 4(d), (e) and (f). The temperature and relative humidity results are taken as the average of nine spatially distributed points, described in Section 2.3, with the effect of the spatial distribution of the temperature and relative humidity measurements elucidated in Section 3.2.

Fig. 4(a), (b) and (c) demonstrate a consistent dependence of the shrinkage on the water to binder ratio, with increases in w/b generally resulting in increases in the measured shrinkage. Initially, it might be expected that smaller water contents lead to higher shrinkage as experienced with high strength concretes [15,50], however this no longer holds true at the low w/b ratios used to manufacture UHPC in this study.

The higher measured shrinkage with w/b in this test program appears to be opposite to the findings in [5,9], who show reduced shrinkage with w/b. However, these differences in observations may be due to different selection of reference time, the shrinkage data presented in this paper is measured starting from 3 h after water addition in contrast to [9] where the results are given after 24 h. This is important because both autogenous shrinkage and converted chemical shrinkage are present in the data in Fig. 4(a), (b) and (c), whereas the converted chemical shrinkage will likely be absent from the data in [9].

There are two distinct peaks in the measured temperature change shown in Fig. 4(d), (e) and (f). The second of these peaks, termed 'shoulder peak' [51], occurs at approximately 40 h after water addition. This peak can be explained by the heat release caused by aluminate hydration, with the main hydration product being ettringite [51]. As shown in Fig. 4(a), (b) and (c) this reaction results in chemical expansion, with the maximum temperature variation being smaller than 2℃ thermal expansion is likely to be negligible in comparison with the magnitudes of shrinkage. The expansive strains and shoulder peaks of higher w/b samples in this study are larger than those of the lower w/b samples and may be due to the greater water availability for the dissolution of sulphate, in turn enabling higher ettringite formation.

It can be seen from Fig. 4(a), (b) and (c), that higher silica fume dosage decreases the shrinkage, this is same as the results observed for UHPC paste [52]. The corresponding temperature change is shown in Fig. 4(d), (e) and (f). The first temperature peak occurring at approximately 20 h after water addition represents the exothermic reaction of alite (C_3S) [51]. It can be seen that a larger silica fume dosage decreases the value of the first peak.

The relative humidity change in Fig. 4(d), (e) and (f) demonstrate a consistent trend that the greater the water to binder ratio, the smaller the gradient of the relative humidity reduction. In approximately the first 15 h after water addition, the relative humidity of all mix designs increases to reach stabilisation, as the relative humidity value of UHPC samples is higher than the initial internal environment local to the embedded sensor. This stabilisation process lasts approximately 15 h due to slow stabilisation speed of sensors, which is a common difficulty for relative humidity measurement [53]. Following the relative humidity stabilisation, the first sign of a decrease in the relative humidity appears, similar to the relative humidity decrease commencement time, identified by Zhang, Liu and Wong [26]. However, after several hours decreasing, the relative humidity starts to increase from approximately 24 h to 30 h. The effect of this relative humidity increase on shrinkage is further discussed in Section 4.1. A continuous decrease in the relative humidity is observed after 30 h, with the rate of decrease continuing to slow throughout the entire 168 h recorded.

The relative humidity measured in the tests only begins to descend in Fig. 4(d), (e) and (f) from around 30 h after water addition.

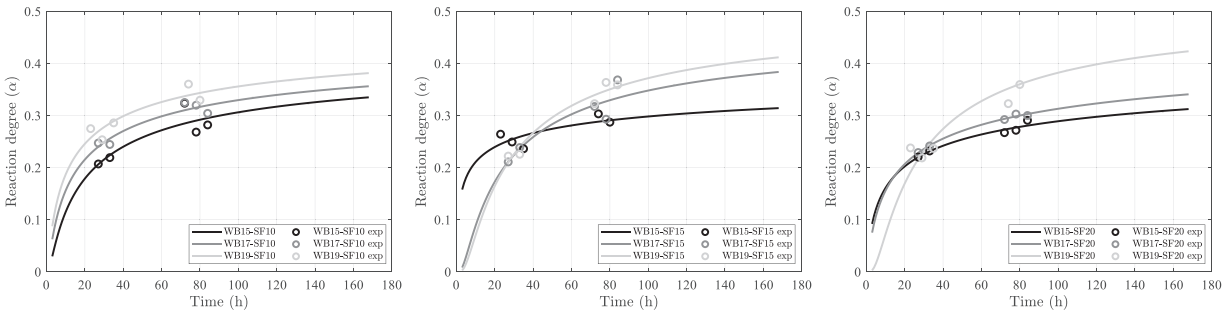

Fig. 8. The effect of water to binder ratio on reaction degree under sealed condition, from 3 h after water addition.

Table 3
Parameters for reaction degree fitting curves.

	WB15-SF10	WB15-SF15	WB15-SF20	WB17-SF10	WB17-SF15	WB17-SF20	WB19-SF10	WB19-SF15	WB19-SF20
α_u	0.430	0.444	0.458	0.460	0.473	0.487	0.485	0.499	0.513
A	5.965	3.398	11.357	11.632	20.190	13.768	9.095	22.658	22.658
B	0.3174	0.2722	0.3563	0.5111	0.7375	0.4109	0.4870	0.8235	0.8235

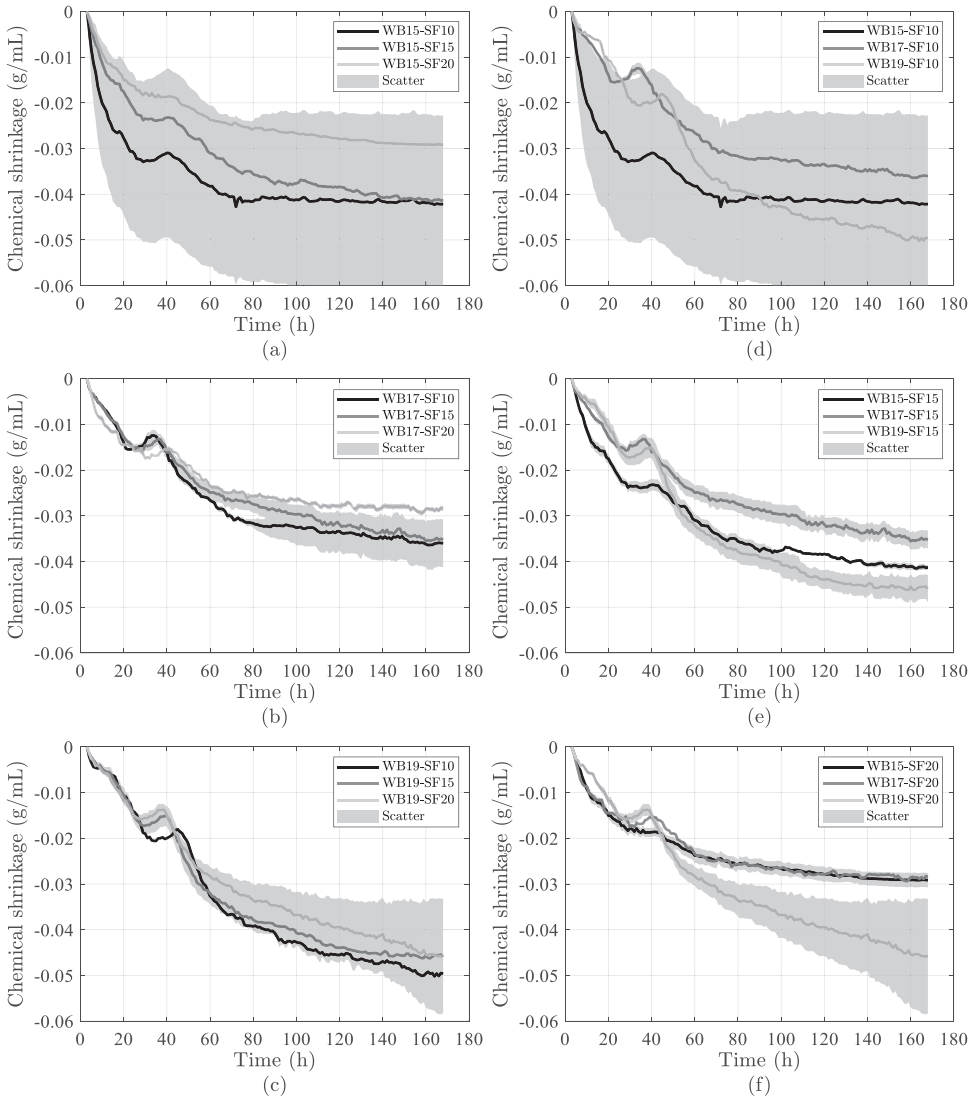

Fig. 9. The effect of silica fume (left) and w/b (right) on chemical shrinkage, recorded from 3 h after water addition.

The rapid shrinkage of the samples in Fig. 4(a), (b) and (c) has already taken place, prior to this RH reduction, thus this shrinkage is not caused by capillary stress. The RH reduction, after ~30 h is accompanied by a steadier and constantly reducing shrinkage rate. The RH has yet to reach equilibrium with the external environment, so further capillary shrinkage would be expected beyond the duration of these tests.

3.1.2. Shrinkage under unsealed boundary condition

In this experimental program, curing conditions were identical for all specimens as they were placed in a temperature and humidity controlled cabinet. However, differences in the ambient temperature and relative humidity during mixing and immediately prior to placement into the temperature and humidity cabinet can affect the unsealed shrinkage in this very early stage.

The effect of different w/b ratios and silica fume dosage on unsealed shrinkage can be seen in Fig. 5(a), (b) and (c) and the

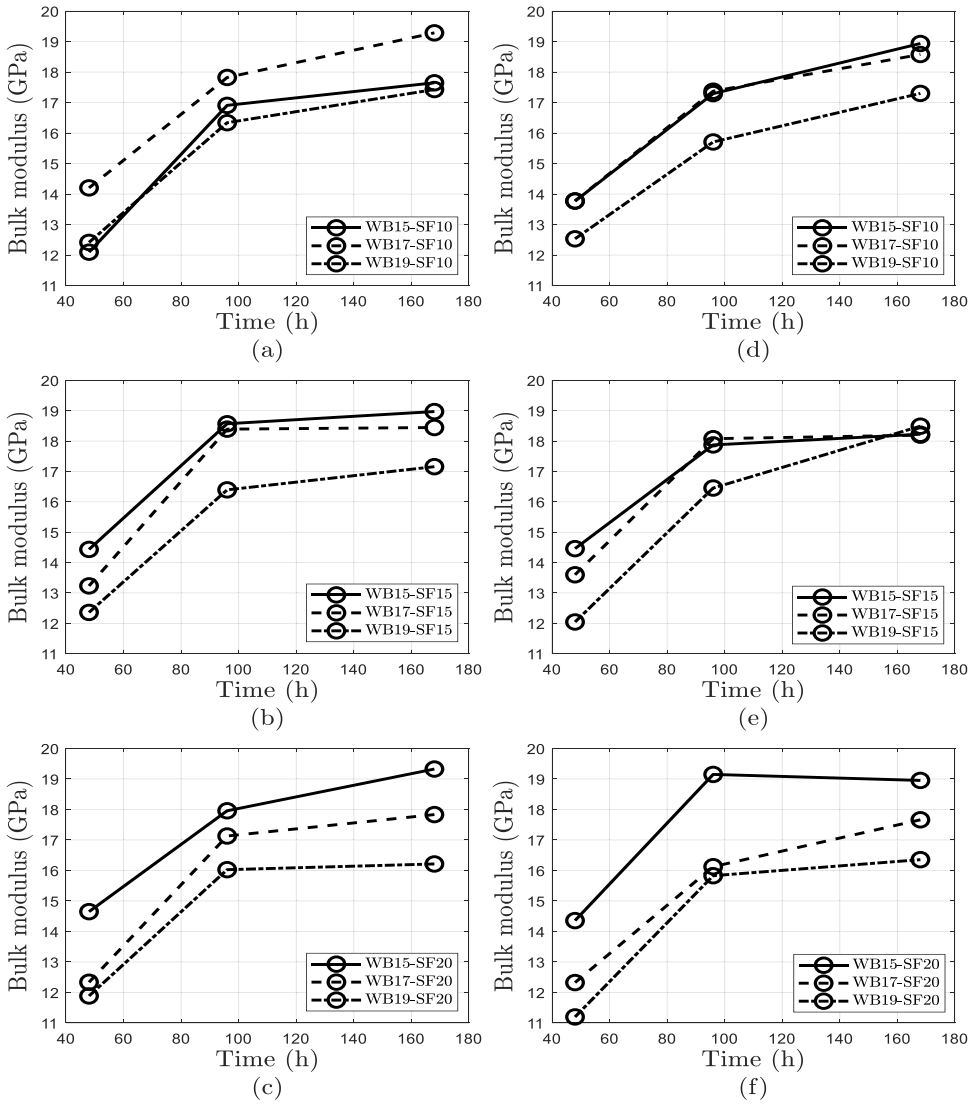

Fig. 10. The effect of w/b on bulk modulus of sealed samples (left) and unsealed samples (right) at 48, 96 and 168 h after water addition.

corresponding temperature and relative humidity can be seen in Fig. 5(d), (e) and (f). Each solid line represents average values of three specimens measured and the grey shaded area is experimental scatter.

As shown in Fig. 5(a), (b) and (c), a greater dosage of silica fume leads to an increase in shrinkage. Research on ordinary strength concrete mortar found that more silica fume can increase drying shrinkage due to pozzolanic reaction and pore size reduction [54]. However, the low water availability of UHPC with low w/b ratios can limit cement hydration and then further limit pozzolanic reaction of silica fume, which may restrict the effect of increasing silica fume on UHPC unsealed shrinkage.

The effect of w/b ratio on unsealed shrinkage, as shown in Fig. 5(a), (b) and (c), is not clear. The major difference in shrinkage between samples with different w/b ratios occurs before 20 h, the difference thereafter is relatively small, as shown in Fig. 5(a), (b) and (c). This may because moisture has greater potential to evaporate in this early period. In addition, the greater chemical shrinkage, resulting from higher w/b ratio, is more likely to convert to external shrinkage during the very early plastic stage, compared with hardened stage, leading to more measured unsealed shrinkage before 20 h. After 20 h, the formation of solid skeleton can hinder chemical shrinkage conversion.

Fig. 5(d), (e) and (f) demonstrate similar patterns of temperature and RH evolution with time as seen with the sealed samples, noteworthy, again being the lack of drying within the pores until after ~30 h. The relative humidity gradients observed in both sealed and unsealed specimens are similar, indicating that self-desiccation dominates relative humidity reduction. The drying conditions do not significantly enhance the reduction of relative humidity over the entire period that measurements were taken.

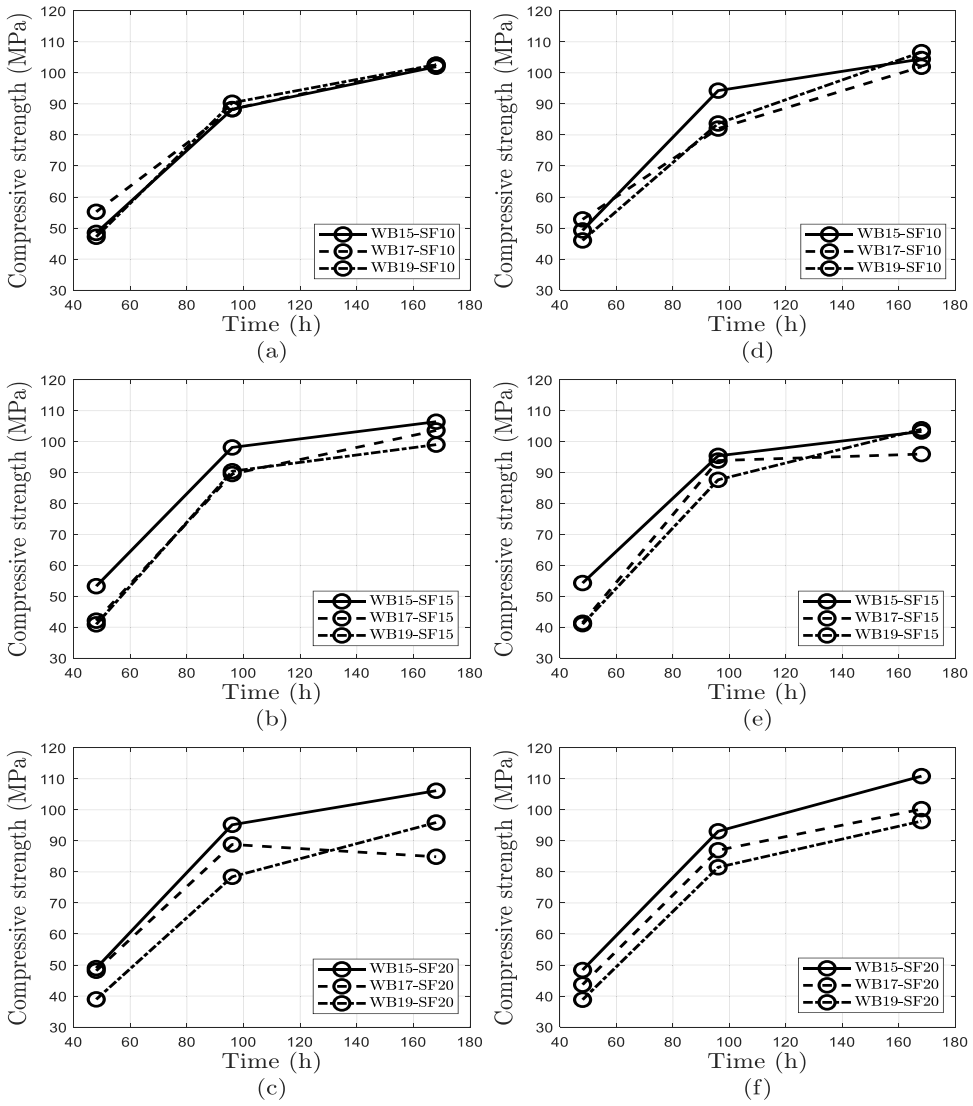

Fig. 11. The effect of w/b on strength of sealed samples (left) and unsealed samples (right) at 48, 96 and 168 h after water addition.

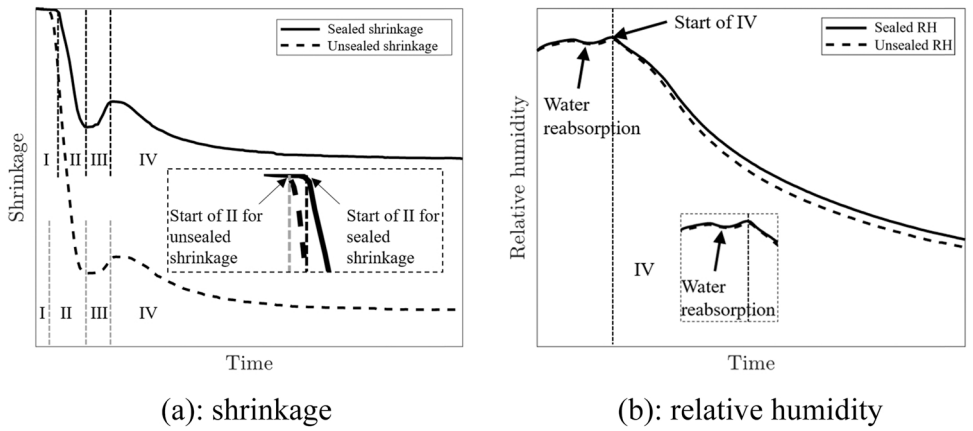

Fig. 12. Schematic representative of shrinkage and relative humidity development patterns.

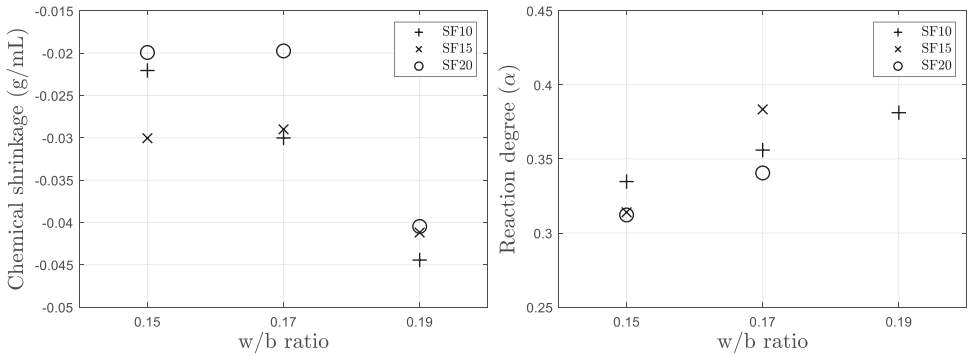

(a): Chemical shrinkage (b): Reaction degree

Fig. 13. Chemical shrinkage (a) and reaction degree (b) at 7 days.

3.1.3. *Comparison between sealed and unsealed shrinkage*

It can be seen, by comparing Figs. 4 and 5, that the major difference in magnitude between sealed and unsealed shrinkage occurred before approximately 20 h. The underlying mechanisms accounting for the difference may be that water evaporation from the sample surface and moisture transport within the sample due to moisture gradient during the entire exposed period [55]; however, the moisture evaporation and transport are more likely to occur before the formation of solid skeleton during the plastic stage, named plastic drying. This may explain why Kang, Hong and Moon [56] observed similar magnitude in UHPC autogenous and total shrinkage, whose shrinkage measurement commenced 12–15 h after water addition.

The effect of drying conditions on UHPC shrinkage after approximately 20 h appears to be limited, as the development in magnitude of sealed and unsealed shrinkage is similar.

3.2. *Spatial distribution of internal temperature and relative humidity*

Fig. 6 shows the spatial and temporal distribution of internal temperature for each mix under sealed and unsealed boundary conditions. The different shades in each graph represent the position of sensors. All of the graphs in Fig. 6 demonstrate that at the two temperature peaks, seen at approximately 20 and 40 h, the temperature recorded by the central sensor is consistently higher than the four edge sensors, which are in turn higher than the four corner sensors. The spatial temperature differential, for both sealed and unsealed specimens, is only of the order of 1℃, but could lead to size effects in larger specimen sizes.

Due to the heat exchange between samples and the environment, the spatial distribution of temperature observed in unsealed samples is smaller than that of the sealed samples. In addition, the initial temperature (at 3 h after water addition) of the unsealed samples is lower than sealed samples, owing to heat losses.

The spatial distribution of relative humidity under sealed moisture transport boundary conditions does not show any overall trend (Fig. 7). The moisture sealing of the samples is likely to also provide thermal insulation as the sensors nearer to the edges in unsealed samples exhibit a sharper decline.

3.3. *Reaction degree*

The degree of reaction α can be expressed by Eq. (4) [43,57,58]:

$$\alpha = \alpha_u e^{(A/t)^B} \tag{4}$$

where t is time, A and B are hydration time parameter and hydration shape parameter, respectively and α_u is ultimate reaction degree [58]. The ultimate reaction degree is governed by the degree of cement hydration and silica fume pozzolanic reaction; however, these two types of chemical reaction are not independent of one another. For example, calcium hydroxide (CH) is one of the cement hydration products dominated by water content and is also required for silica fume reaction. Therefore, both water to cement ratio (w/c) and silica fume to cement ratio (s/c) are essential.

The ultimate reaction degree α_u can be estimated by Eq. (5) [59]:

$$\alpha_u = \frac{1.032w/c - 0.279(s/c)\alpha_{su}}{0.194 + w/c} \tag{5}$$

where α_{su} is the ultimate reaction degree of silica fume and it is related to w/c. For example, when w/c= 0.5, a s/c ratio of 0.16 is required to consume all CH by pozzolanic reaction. If the amount of silica fume is greater than the required value, the excess amount can lessen the ultimate reaction degree of silica fume α_{su} which can be calculated by Eq. (6) [59]:

$$\alpha_{su} = SF^{eff} min\left[1, \frac{(s/c)_{req}}{s/c}\right] \tag{6}$$

In which, $(s/c)_{req}$ is the required s/c to consume all CH, SF^{eff} is the weight ratio of SiO_2 contained in the silica fume because SiO_2 is the effective part that can participate in pozzolanic reaction, while the remaining part plays the role of an inert filler. The SF^{eff} of silica fume used in this research is 89.6%, based on the product data sheet [36].

For concrete with different w/c, the required s/c to consume all CH can be calculated by Eq. (7) [59]:

$$(s/c)_{req} = \min(0.16, 0.4w/c) \tag{7}$$

The effect of water to binder ratio on reaction degree is shown in Fig. 8. The solid lines represent fitted curves given by Eq. (4) and the circles are experimental results, obtained by Eq. (2). The values for fitting parameters in Eq. (4) can be seen in Table 3. All graphs in Fig. 8 demonstrate that, beyond 80 h, greater water to binder ratios result in an increased reaction degree.

3.4. Chemical shrinkage

The chemical shrinkage values measured by Erlenmeyer flask and pipette as described in Section 2.5 are shown in Fig. 9. The effect of silica fume dosages with constant w/b ratio on chemical shrinkage can be seen in Fig. 9(a), (b) and (c). The effect of w/b ratios with constant silica fume dosage on chemical shrinkage can be seen in Fig. 9(d), (e) and (f). Each solid line is average values of two measured specimens and the grey shaded area is experimental scatter.

It can be seen that when w/b ratio remains constant, greater silica fume dosage decreases chemical shrinkage and when silica fume dosage remains constant, larger w/b ratio increases chemical shrinkage. These observations are the same as sealed shrinkage, as described in Section 3.1.1, indicating chemical shrinkage conversion may be one of the factors that affects sealed shrinkage development.

The chemical shrinkage in the first $\sim$ 30 h has a large scatter in the recordings making it difficult to discern the effect of w/b. Additionally, the amount of this shrinkage that is actually converted to shrinkage of samples in Section 3.1 cannot be directly determined as not all chemical shrinkage is converted to actual shrinkage of specimens as restraint increases with the development of stiffness.

It can be noted that in Fig. 9, expansive strains occur in all of the mixes at approximately 30 h after water addition, similar to the expansion observed in sealed and unsealed shrinkage specimens, as shown in Figs. 4 and 5. Whilst the expansions observed in all of the experiments is due to aluminate hydration, the sealed and unsealed shrinkage experiments are predominantly due to ettringite formation, whereas thermal expansion is prevalent in chemical shrinkage.

In order to accurately measure the volumetric deformation occurring in the Erlenmeyer flask, the volumetric difference between the Erlenmeyer flask and the pipette is large, leading to high sensitivity of volume change. In addition, the volume of paraffin oil in the Erlenmeyer flask is much larger than the sample; therefore, the volume change resulting from the exothermic reactions comes mainly from paraffin oil rather than the sample. Although the test data picked up this expansive strain, the overall chemical shrinkage development is accurate.

3.5. Bulk modulus and compressive strength

The effect of water to binder ratios on bulk modulus of sealed samples can be seen in Fig. 10(a), (b) and (c), and unsealed samples in Fig. 10(d), (e) and (f). A smaller water to binder ratio consistently results in greater bulk modulus.

The corresponding strength of sealed and unsealed samples, considering the effect of water to binder ratio is shown in Fig. 11(a)–(c) and (d)–(f), respectively. Similar to bulk modulus, all graphs in Fig. 11 demonstrate that lower water to binder ratio results in higher compressive strength. This may be because the denser packaging of specimens with smaller water to binder ratio can improve bulk modulus and compressive strength in the first 7 days, although the reaction degree is lower.

4. Discussion

4.1. Shrinkage mechanisms

The test results for both sealed (Fig. 4) and unsealed shrinkage (Fig. 5) appear to show that the shrinkage occurs in four phases, as schematically illustrated in Fig. 12(a) representative of the data presented in Section 3.1. Fig. 13(b) schematically shows the corresponding changes in relative humidity reflecting the data presented in Section 3.3.

The four stages identified are:

- Stage I (plastic settlement stage): Up to approximately 15 h after casting, the UHPC specimens are in their plastic stage, whereby the shape rigidity is not sufficient to support its own weight. The deformation that occurs in this stage may be predominantly vertical settlement and the horizontal deformation is relatively small in comparison [60]. The end time of this initial stage differs slightly between sealed and unsealed conditions.

- Stage II (rapid shrinkage stage): The shrinkage strain increases rapidly during this stage and accounts for approximately 70% of shrinkage in the first 7 days. The dominant mechanism in sealed samples is the chemical shrinkage resulting from hydration [15, 16] with little autogenous shrinkage contribution as demonstrated by the relatively constant internal relative humidity, as shown schematically in Fig. 12(b) this is similar to findings presented in [16]. In unsealed samples, both chemical shrinkage and evaporation can occur, with the major difference in the magnitude of measured shrinkage taking place in this stage, as shown schematically in Fig. 12(a). The differences in sealed and unsealed shrinkage presumably result from the evaporation of mix water, in the unsealed samples, as they equilibrate with the humidity of the environmental chamber.

- Stage III (expansion stage): An expansion phase is observed, as shown in Fig. 12(a), caused by a combination of ettringite formation [22,26,51,61] and water absorption, as shown in Fig. 12(b). The expansion of unsealed samples is slightly smaller than that of sealed samples.
- Stage IV (moderate shrinkage stage): This stage is identified as the recommencement of shrinkage. The relative humidity descends from this time and represents the beginning of capillary-related shrinkage, as shown in Fig. 12(b). As shown in Fig. 12(a), the magnitude of shrinkage of both sealed and unsealed specimens is very similar, and as shown in Fig. 12(b), the relative humidity difference between sealed and unsealed samples is negligible, thereby demonstrating the limited effect of pore drying in this stage.

The delay between shrinkage development in stage II and the beginning of the descent of RH in stage IV indicates that chemical shrinkage dominates stage II. This observation differs slightly with Zhang, Liu and Wang [26] who observed simultaneous drops in relative humidity and shrinkage.

The observation of the effect of silica fume on sealed shrinkage in this test is opposite to the findings in [9] who hypothesise that silica fume can reduce pore sizes and contribute to shrinkage development. This may because the inadequate distribution and agglomeration of silica fume particles, resulting from high silica fume content can lead to higher porosity [62]; in addition, densified silica fume with larger particle size distribution was used in this test, which may have led to limited porosity reduction [63]. Silica fume can absorb water and reduce that available for cement hydration; moreover, silica fume particles can form a barrier layer surrounding cement particle to hinder the contact between water and cement [64]. Silica fume can therefore work as retarder to hinder cement hydration, resulting in less calcium hydroxide (*CH*) available for the pozzolanic reaction of silica fume, which may also be the reason for the reduced first peak value of temperature with increased silica fume dosage. It is therefore suggested that further study of this phenomena is required.

4.2. Chemical shrinkage and reaction degree

Chemical shrinkage occurs as a result of chemical reaction; therefore, it is closely correlated to reaction degree. The final values of reaction degree and chemical shrinkage at 7 days are compared in Fig. 13. The different shaped data points represent different silica fume replacement ratios. The full reaction degree change data can be seen in Section 3.3.

It can be seen in Fig. 13 that when w/b ratio increases, both chemical shrinkage and reaction degree increase, due to more water content for chemical reaction. Greater silica fume replacement decreases the development of both chemical shrinkage and the reaction degree. This further demonstrates the retardation effect of silica fume on chemical reaction, as stated in Section 4.1.

5. Conclusions

Experimental investigations of shrinkage of UHPC have shown that the early age volume changes are significant, this is in contrast to shrinkage in normal and high strength concrete which predominately occurs at later ages as a result of drying. An understanding of the role of the individual components of UHPC mix designs in early age shrinkage is essential for mix design. Furthermore, to ensure adequate performance at later ages, the effect of the shrinkage that occurs in these early stages on the formation of permanent defects needs to be understood.

While an increasing dataset of UHPC total and autogenous shrinkage strains at later ages is available, very little testing has been conducted at very early ages and to date the role of water to binder ratio and binder composition is not well understood. To address this limitation, and to provide detailed test results for future model development, in this paper the results of detailed early age shrinkage experiments on UHPC with varying water to binder ratio and various quantities of silica fume are presented.

The outcomes of this experimental research have led to the following conclusions:

- An increasing w/b ratio leads to a clear increase in shrinkage in sealed specimens, the correlation is not so clear in unsealed conditions owing to significant experimental scatter. Shrinkage under both boundary conditions is seen to be directly proportional to the silica fume dosage.
- It is demonstrated that shrinkage occurring during stage II dominates the 7 days shrinkage of UHPC. Under sealed conditions, this shrinkage is governed by chemical shrinkage conversion and under unsealed conditions, this shrinkage is due to chemical shrinkage conversion and moisture evaporation.
- Shrinkage occurring after stage II accounts for a small part of 7-day early-age shrinkage. The magnitudes of this shrinkage for sealed and unsealed shrinkage are almost the same, indicating a limited drying effect

- Spatial variability in measured internal temperatures could be indicative of shrinkage size effects that could be become particularly prevalent in member sizes larger than laboratory specimens and further research is required to investigate the influence of specimen size.

Declaration of Competing Interest

The authors declare that they have no known competing financial interests or personal relationships that could have appeared to influence the work reported in this paper.

Acknowledgements

This material is based upon work supported by Australian Research Council Discovery Project 190102650. The first author would additionally like to thank The University of Adelaide for providing financial support through an Adelaide Graduate Research Scholarship.

References

[1] E. Ghafari, S.A. Ghahari, H. Costa, E. Júlio, A. Portugal, L. Durães, Effect of supplementary cementitious materials on autogenous shrinkage of ultra-high performance concrete, Constr. Build. Mater. 127 (2016) 43–48.
[2] H. Huang, G. Ye, Examining the "time-zero" of autogenous shrinkage in high/ultra-high performance cement pastes, Cem. Concr. Res. 97 (2017) 107–114.
[3] W. Li, Z. Huang, G. Hu, W.H. Duan, S.P. Shah, Early-age shrinkage development of ultra-high-performance concrete under heat curing treatment, Constr. Build. Mater. 131 (2017) 767–774.
[4] C. Shi, Z. Wu, J. Xiao, D. Wang, Z. Huang, Z. Fang, A review on ultra high performance concrete: part I. Raw materials and mixture design, Constr. Build. Mater. 101 (2015) 741–751.
[5] D. Wang, C. Shi, Z. Wu, J. Xiao, Z. Huang, Z. Fang, A review on ultra high performance concrete: part II. Hydration, microstructure and properties, Constr. Build. Mater. 96 (2015) 368–377.
[6] T. Xie, C. Fang, M.M. Ali, P. Visintin, Characterizations of autogenous and drying shrinkage of ultra-high performance concrete (UHPC): an experimental study, Cem. Concr. Compos. 91 (2018) 156–173.
[7] O.M. Jensen, P.F. Hansen, Autogenous deformation and RH-change in perspective, Cem. Concr. Res. 31 (12) (2001) 1859–1865.
[8] D. Shen, J. Jiang, J. Shen, P. Yao, G. Jiang, Influence of curing temperature on autogenous shrinkage and cracking resistance of high-performance concrete at an early age, Constr. Build. Mater. 103 (2016) 67–76.
[9] P. Shen, L. Lu, Y. He, M. Rao, Z. Fu, F. Wang, S. Hu, Experimental investigation on the autogenous shrinkage of steam cured ultra-high performance concrete, Constr. Build. Mater. 162 (2018) 512–522.
[10] A. Soliman, M. Nehdi, Effect of partially hydrated cementitious materials and superabsorbent polymer on early-age shrinkage of UHPC, Constr. Build. Mater. 41 (2013) 270–275.
[11] O.M. Jensen, Autogenous Deformation and RH-Change—self-desiccation and Self-desiccation Shrinkage, Building Materials Laboratory, The Technical University of Denmark, Lyngby, Denmark, 285, 1993, p. 93.
[12] J. Liu, N. Farzadnia, C. Shi, X. Ma, Effects of superabsorbent polymer on shrinkage properties of ultra-high strength concrete under drying condition, Constr. Build. Mater. 215 (2019) 799–811.
[13] E. Holt, M. Leivo, Cracking risks associated with early age shrinkage, Cem. Concr. Compos. 26 (5) (2004) 521–530.
[14] Bt Bissonnette, P. Pierre, M. Pigeon, Influence of key parameters on drying shrinkage of cementitious materials, Cem. Concr. Res. 29 (10) (1999) 1655–1662.
[15] E. Holt, Contribution of mixture design to chemical and autogenous shrinkage of concrete at early ages, Cem. Concr. Res. 35 (3) (2005) 464–472.
[16] P. Lura, O.M. Jensen, K. Van Breugel, Autogenous shrinkage in high-performance cement paste: an evaluation of basic mechanisms, Cem. Concr. Res. 33 (2) (2003) 223–232.
[17] Y. Luan, T. Ishida, Enhanced shrinkage model based on early age hydration and moisture status in pore structure, J. Adv. Concr. Technol. 11 (12) (2013) 360–373.
[18] K. Kovler, S. Zhutovsky, Overview and future trends of shrinkage research, Mater. Struct. 39 (9) (2006) 827–847.
[19] C. Hua, P. Acker, A. Ehrlacher, Analyses and models of the autogenous shrinkage of hardening cement paste: I. Modelling at macroscopic scale, Cem. Concr. Res. 25 (7) (1995) 1457–1468.
[20] S. Eppers, C. Müller, Autogenous shrinkage strain of ultra-high-performance concrete (UHPC), in: Proceedings of the 2nd International Symposium on UHPC, Kassel, Germany, 2008, pp. 433–441.
[21] J.J. Park, D.Y. Yoo, S.W. Kim, Y.S. Yoon, Autogenous shrinkage of ultra high performance concrete considering early age coefficient of thermal expansion, Struct. Eng. Mech. 49 (6) (2014) 763–773.
[22] Ç. Yalçınkaya, H. Yazıcı, Effects of ambient temperature and relative humidity on early-age shrinkage of UHPC with high-volume mineral admixtures, Constr. Build. Mater. 144 (2017) 252–259.
[23] J. Liu, C. Shi, Z. Wu, Hardening, microstructure, and shrinkage development of UHPC: a review, J. Asian Concr. Fed. 5 (2) (2019) 1–19.
[24] P. Termkhajornkit, T. Nawa, M. Nakai, T. Saito, Effect of fly ash on autogenous shrinkage, Cem. Concr. Res. 35 (3) (2005) 473–482.
[25] E.-i Tazawa, Autogenous Shrinkage of Concrete, CRC Press, 1999.
[26] X. Zhang, Z. Liu, F. Wang, Autogenous shrinkage behavior of ultra-high performance concrete, Constr. Build. Mater. 226 (2019) 459–468.
[27] Z. Wu, C. Shi, K.H. Khayat, Investigation of mechanical properties and shrinkage of ultra-high performance concrete: influence of steel fiber content and shape, Compos. Part B Eng. 174 (2019), 107021.
[28] J.-Y. Wang, C. Bian, R.-C. Xiao, B. Ma, Restrained shrinkage mechanism of ultra high performance concrete, KSCE J. Civ. Eng. 23 (10) (2019) 4481–4492.
[29] Z. Liu, S. El-Tawil, W. Hansen, F. Wang, Effect of slag cement on the properties of ultra-high performance concrete, Constr. Build. Mater. 190 (2018) 830–837.
[30] R. Yang, R. Yu, Z. Shui, X. Gao, X. Xiao, X. Zhang, Y. Wang, Y. He, Low carbon design of an ultra-high performance concrete (UHPC) incorporating phosphorous slag, J. Clean. Prod. 240 (2019), 118157.
[31] R. Yang, R. Yu, Z. Shui, X. Gao, J. Han, G. Lin, D. Qian, Z. Liu, Y. He, Environmental and economical friendly ultra-high performance-concrete incorporating appropriate quarry-stone powders, J. Clean. Prod. 260 (2020), 121112.
[32] J.L. Lim, S.N. Raman, M. Safiuddin, M.F.M. Zain, R. Hamid, Autogenous shrinkage, microstructure, and strength of ultra-high performance concrete incorporating carbon nanofibers, Materials 12 (2) (2019) 320.
[33] AS 3972-2010 General Purpose and Blended Cements, Standards Australia, 2010.
[34] AS/NZS 3582.3:2016 Supplementary Cementitious Materials, Part 3: Amorphous silica, Standards Australia/Standards New Zealand, 2016.
[35] Product Data Sheet Sulfate Resisting Cement, Adelaide Brighton Cement Ltd, 2018.
[36] ECOTEC Silica Fume Datasheet, ECOTEC Silica Fume, 2012.

[37] V. Slowik, M. Schmidt, R. Fritzsch, Capillary pressure in fresh cement-based materials and identification of the air entry value, Cem. Concr. Compos. 30 (7) (2008) 557–565.
[38] G. Olivier, R. Combrinck, M. Kayondo, W.P. Boshoff, Combined effect of nano-silica, super absorbent polymers, and synthetic fibres on plastic shrinkage cracking in concrete, Constr. Build. Mater. 192 (2018) 85–98.
[39] E.E. Holt, Early Age Autogenous Shrinkage of Concrete, Technical Research Centre of Finland Espoo, Finland, 2001.
[40] S. Staquet, B. Espion, Early age autogenous shrinkage of UHPC incorporating very fine fly ash or metakaolin in replacement of silica fume, in: Proceedings of the International Symposium on Ultra High Performance Concrete, Kessel Germany, 2004, pp. 587–599.
[41] Z. Jun, H. Dongwei, C. Haoyu, Experimental and theoretical studies on autogenous shrinkage of concrete at early ages, J. Mater. Civ. Eng. 23 (3) (2010) 312–320.
[42] D. Cusson, T. Hoogeveen, An experimental approach for the analysis of early-age behaviour of high-performance concrete structures under restrained shrinkage, Cem. Concr. Res. 37 (2) (2007) 200–209.
[43] J. Zhang, D. Hou, Y. Han, Micromechanical modeling on autogenous and drying shrinkages of concrete, Constr. Build. Mater. 29 (2012) 230–240.
[44] S. Monteagudo, A. Moragues, J. Gálvez, M. Casati, E. Reyes, The degree of hydration assessment of blended cement pastes by differential thermal and thermogravimetric analysis. Morphological evolution of the solid phases, Thermochim. Acta 592 (2014) 37–51.
[45] W. Deboucha, N. Leklou, A. Khelidj, M.N. Oudjit, Hydration development of mineral additives blended cement using thermogravimetric analysis (TGA): methodology of calculating the degree of hydration, Constr. Build. Mater. 146 (2017) 687–701.
[46] ASTM, C1608-07 Standard Test Method for Chemical Shrinkage of Hydraulic Paste, American Society for Testing and Materials and Structures, 2007.
[47] T. Zhang, P. Gao, R. Luo, Y. Guo, J. Wei, Q. Yu, Measurement of chemical shrinkage of cement paste: comparison study of ASTM C 1608 and an improved method, Constr. Build. Mater. 48 (2013) 662–669.
[48] ASTM, C39/C39M-10 Standard Test Method for Compressive Strength of Cylindrical Concrete Specimens, American Society for Testing and Materials and Structures, 2010.
[49] ASTM, C469/C469M-10 Standard Test Method for Static Modulus of Elasticity and Poisson's Ratio of Concrete in Compression, American Society for Testing and Materials and Structures, 2010.
[50] Z. Jiang, Z. Sun, P. Wang, Autogenous relative humidity change and autogenous shrinkage of high-performance cement pastes, Cem. Concr. Res. 35 (8) (2005) 1539–1545.
[51] J.W. Bullard, H.M. Jennings, R.A. Livingston, A. Nonat, G.W. Scherer, J.S. Schweitzer, K.L. Scrivener, J.J. Thomas, Mechanisms of cement hydration, Cem. Concr. Res. 41 (12) (2011) 1208–1223.
[52] P.R. Rangaraju, Z. Li, Development of UHPC using ternary blends of ultra-fine class F fly ash, meta-kaolin and portland cement, in: Proceedings of the International Interactive Symposium on Ultra-High Performance Concrete, Iowa State University Digital Press, 2016.
[53] C. Andrade, J. Sarría, C. Alonso, Relative humidity in the interior of concrete exposed to natural and artificial weathering, Cem. Concr. Res. 29 (8) (1999) 1249–1259.
[54] G.A. Rao, Long-term drying shrinkage of mortar—influence of silica fume and size of fine aggregate, Cem. Concr. Res. 31 (2) (2001) 171–175.
[55] Z.P. Bažant, M. Jirásek. Creep and Hygrothermal Effects in Concrete Structures, Springer, 2018.
[56] S.-H. Kang, S.-G. Hong, J. Moon, Shrinkage characteristics of heat-treated ultra-high performance concrete and its mitigation using superabsorbent polymer based internal curing method, Cem. Concr. Compos. 89 (2018) 130–138.
[57] A.K. Schindler, K.J. Folliard, Heat of hydration models for cementitious materials, Acids Mater. J. 102 (1) (2005) 24.
[58] I. Pane, W. Hansen, Concrete hydration and mechanical properties under nonisothermal conditions, Mater. J. 99 (6) (2002) 534–542.
[59] G. Di Luzio, G. Cusatis, Hygro-thermo-chemical modeling of high performance concrete. I: theory, Cem. Concr. Compos. 31 (5) (2009) 301–308.
[60] S. Ghourchian, M. Wyrzykowski, P. Lura, A poromechanics model for plastic shrinkage of fresh cementitious materials, Cem. Concr. Res. 109 (2018) 120–132.
[61] J. Beaudoin, I. Odler, Hydration, setting and hardening of Portland cement. Lea's Chemistry of Cement and Concrete, fifth ed., Butterworth-Heinemann, Oxford, 2019, pp. 157–250.
[62] A. Soliman, M. Nehdi, Effect of drying conditions on autogenous shrinkage in ultra-high performance concrete at early-age, Mater. Struct. 44 (5) (2011) 879–899.
[63] S. Diamond, S. Sahu, Densified silica fume: particle sizes and dispersion in concrete, Mater. Struct. 39 (9) (2006) 849–859.
[64] B. Langan, K. Weng, M. Ward, Effect of silica fume and fly ash on heat of hydration of Portland cement, Cem. Concr. Res. 32 (7) (2002) 1045–1051.